INSTITUTE OF PHYSICS PUBLISHING NANOTECHNOLOGY
Nanotechnology **16** (2005) 186–198 doi:10.1088/0957-4484/16/2/003

# The oscillatory damped behaviour of incommensurate double-walled carbon nanotubes

**José L Rivera[1], Clare McCabe[2] and Peter T Cummings[2,3]**

[1] Department of Chemical Engineering, Universidad Michoacana de San Nicolás de Hidalgo, Santiago Tapia No. 403, Colonia Centro, Morelia, Michoacan 58000, Mexico
[2] Department of Chemical Engineering, Vanderbilt University, Nashville, TN 37235-1604, USA
[3] Chemical Sciences Division, Oak Ridge National Laboratory, TN 37831-6110, USA

E-mail: peter.t.cummings@vanderbilt.edu

Received 16 August 2004, in final form 19 November 2004
Published 23 December 2004
Online at stacks.iop.org/Nano/16/186

**Abstract**
The mechanical properties of sliding carbon nanotubes have been investigated by classical molecular dynamics simulations in the canonical ensemble. In particular we have studied damped oscillations in the separation between the centres of mass of the inner and outer tubes of double-walled carbon nanotubes (DWCN). Incommensurate DWCNs forming (7, 0)@(9, 9) structures were simulated for systems at 298.15 K with axial lengths from 12.21 to 98.24 nm. The oscillations exhibited frequencies in the range of gigahertz with the frequency decreasing as the length of the system increases. The time until oscillations become negligible exhibited a nearly linear dependence on the length of the system. Two macroscopic models were developed in order to understand the forces involved in terms of macroscopic properties like friction and shear. The first model considered constant restoring forces during the whole event, while in the second the value of these constant restoring forces depended on the initial conditions of each oscillation. Both models reproduced the oscillations quite well, while the second model allows us to predict the dynamic shear strength in terms of the axial length of the system for tubes with the same diameters. The calculated dynamic shear strength exhibited monotonic behaviour with an inverse dependence on the length of the system. For systems with unequal axial lengths, the restoring force, which drives the oscillation, is reduced compared to the system with equal lengths, regardless of whether the outer nanotube is longer or shorter.

M This article contains online multimedia enhancements

## 1. Introduction

Theoretical research on nanoscale devices has rapidly grown in recent years [1–4]. It is expected that these devices will enable the realization of miniature versions of electronic integrated circuits and mechanical systems [5], which will process precisely, efficiently and with high productivity, matter, energy and information [6]. Research has primarily focused on structures that require precise control over the positioning of molecular systems in order to be built and perform the activities for which they were developed [7]. Technologies to manipulate such systems are in the very early stage of development [8–10], and include atomic force microscopy (AFM), and high-resolution transmission (TEM) and scanning (SEM) electron microscopy techniques, which are used to quantify and verify the mechanical properties of nanoscale structures. Multi-walled carbon nanotubes (MWCN) constitute a

promising class of nano-materials, which has the appropriate structure and properties to build nanoscale devices [2, 5, 11].

The technology to create carbon nanotubes has been known for more than a decade [12]; however, the experimental parameters that influence nanotube formation and control of the outer diameter, number of shells, internal conformation and axial length remain under investigation [13–15]. Using chemical vapour deposition over catalytic nanoparticles of discrete sizes, Li *et al* [13] have produced carbon nanotubes with diameters close to the size of the catalytic nanoparticles. The nanoparticles employed were made of iron oxide, and were put in contact with methane and hydrogen at 1173 K. This resulted in nanotubes with axial lengths in the range 0.01–10 $\mu$m, and outer diameters in the range 1–2, and 3–5 nm, depending on the size of the nanoparticles. Suh and Lee [15] have prepared uniform arrays of carbon nanotubes supported on porous anodic alumina through an electrochemical process. This process uses the anodic alumina as a template where cobalt is deposited at the bottom of the template, reduced and put in contact with pyrolized acetylene to form well ordered nanotubes with highly uniform outer diameters (43.8$\pm$ 0.8 nm) and lengths, which are confirmed by scanning electron micrographs. Using thermal chemical vapour deposition at atmospheric pressure, Siegal *et al* [14] have growth carbon nanotubes from a nickel film using a mixture of acetylene and nitrogen. These nanotubes have a very uniform outer diameter, which depends exponentially on the temperature employed during the process. Using a temperature of 903 K, this method produces nanotubes with an outer diameter of 5 nm, and 350 nm at 1063 K.

Despite success in controlling the outer diameter, axial length and ordering of nanotubes supported on a surface, limited progress has been made in controlling the internal conformation of each wall in the system, which is the most important parameter in determining electric and mechanical phenomena. The internal conformation is characterized by the chiral indices $(n, m)$. These indices dictate in which direction the graphite sheet is bent and rolled over to form the nanotube [16]. Nanotubes can be either of the armchair ($n = m$), zigzag ($n = 0$, or $m = 0$), or chair (any other $n$ and $m$) variety. This internal conformation can be determined experimentally using scanning tunnelling microscopy for single-walled carbon nanotubes [17, 18], but for DWCNs and MWCNs this method cannot be employed. Combining transmission electron microscopy and electron diffraction techniques, recently Kociak *et al* [19] have been able to deduce the chiral indices of each nanotube in DWCN structures, but experimental methods that can produce nanotubes with specific chiral indices have not yet been reported in the literature.

Among the interesting mechanical properties exhibited by DWCNs, superlubricity (very low friction forces compared to graphite) between their walls has been predicted theoretically [20–22]. Using calculations of the corrugation energy, Damnjanovic *et al* [20] have predicted that, in general, the friction between the walls will be extremely low in MWCNs, and superlubricity is present for the case of incommensurate systems. This is a consequence of the low symmetry, or even complete disorder, between the walls in these systems. For any DWCN $(n, m)@(n', m')$ structure, typically they will be incommensurate (but not always) if $n/m \neq n'/m'$, and commensurate if $n/m = n'/m'$ [21]. Using the same type of calculations, Kolmogorov and Crespi [22] have estimated that the shear strength will be $\sim$1 MPa for the commensurate systems where the corrugation energy scales with the size of the system and for incommensurate systems they find that the corrugation energy does not scale with size and the shear strength is ill defined. For simulation purposes, the internal conformations of MWCNs can be chosen in order to produce systems that fall into the commensurate or incommensurate definitions.

There have been several theoretical, simulation and experimental studies of friction forces between surfaces at the atomic scale [23–25], dealing with the commensurability of the surfaces. Using molecular dynamics simulations of curved, non-adhering, dry surfaces, Wenning and Muser [23] found different behaviour for the friction force $F_f$ in commensurate, incommensurate and amorphous systems with respect to the normal load $L$. For commensurate systems the dependence was found to be linear in the load, i.e. $F_f \approx L$; for amorphous systems $F_f \approx L^{0.66}$; for incommensurate systems the dependence was not clear, similar to the conclusion of Kolmogorov and Crespi [22] for nanotube surfaces. If these incommensurate surfaces are contaminated with small lubricant molecules, then the dependence between the friction force and the normal load is well behaved, and $F_f \approx L^{0.85}$. Muser and Robbins [24] have also studied flat commensurate and incommensurate atomically smooth surfaces; they found that commensurate surfaces hold together at zero lateral force and positive normal pressures, while incommensurate surfaces hold together at zero lateral force only when mobile atoms are present in the interface between the surfaces or if the walls are particularly soft. Super-low friction has been observed experimentally in molybdenum disulphide coatings at high vacuum conditions, and in the presence of nitrogen atmospheres [25]. They conclude that the presence of carbon, water or oxygen increase the value of the shear strength, which at atmospheric air conditions is 56.0 MPa, while at ultra high vacuum conditions this decreased to 0.7 MPa. In the case of DWCNs, generally there is no possibility for molecules or atoms to be located between the walls that form the system because the intershell distance is 0.34 nm (same as graphite), which corresponds to the van der Waals diameter for carbon–carbon interactions.

The friction force between the outer surfaces of carbon nanotubes with other material surfaces has been the focus of several molecular simulation studies [26–28]. For example, the sliding and rolling of carbon nanotubes on a graphite surface has been studied by Buldum and Lu [26], who found that each set of chiral indices of a nanotube have a unique minimum energy orientation with respect to the graphite surface. If the nanotube is pushed in any direction along the graphite surface, the nanotube not only slides but also spins looking for a new energy minimum. Using molecular dynamics simulations, Ni and Sinnott [27] studied the responses of bundles of carbon nanotubes to shear forces between two sliding hydrogen-terminated diamond forces. They used an analytic reactive empirical bond-order potential developed by Brenner [29], coupled to a long-range Lennard-Jones potential [30], and found that the shear forces are relatively weak at low compression levels ($\sim$0 GPa) of the

diamond surfaces. At high compression levels (13.7 GPa), the nanotubes bend in the radial direction, producing forces three orders of magnitude higher than the system at low compression levels. Brenner's potential [29] was also used by Frankland *et al* [28] to study the carbon nanotube–polymer interface for cases when the nanotube was not linked to the polymer and when the nanotube formed cross-links involving ∼1% of the nanotube carbon atoms. For carbon nanotubes with chiral indices (10, 10) and a length of 5.3 nm, they found that when the nanotube was not linked, the shear strength is ∼2.75 MPa independent of where the polymer formed a crystalline or amorphous matrix; for the case when the nanotube was linked to the matrix, the shear strength was 30 MPa for an amorphous matrix, and 110 MPa for the crystalline matrix.

Composite materials of carbon nanotubes and metals [31], polymers [32, 33] and fullerenes [34] have been the subject of several molecular simulation and experimental studies. Using a copper matrix reinforced with carbon nanotubes, Dong *et al* [31] found experimentally that the coefficient of friction decreased with the volume fraction content of carbon nanotubes in the composite. When the content of carbon nanotubes changed from 4 to 20%, the friction coefficient decreased from 0.39 to 0.29. The effect is larger for the matrix carbon-reinforced/copper, where on changing the nanotubes volume fraction from 0.04 to 0.20%, the coefficient of friction decreased from 0.43 to 0.29. Carbon nanotube-reinforced epoxy thin films have been investigated experimentally by Xu *et al* [32], and using molecular mechanics simulations and micromechanics calculations. They found that strong interfacial adhesion exists using very low volume fractions of MWCNs. Similar behaviour was also found by Liao and Li [33] in their simulations of carbon nanotube–polystyrene composites. The shear strength of carbon nanotube–fullerene composites was estimated experimentally by Kuzumaki *et al* [34] and, contrary to the behaviour with polymers composites, this interface showed a shear strength of 0.044 MPa. The shear sliding observed is probably caused by the weak bonding between these surfaces.

As shown by Damnjanovic *et al* [20], carbon nanotubes in general exhibit extremely low friction forces between their nested walls. The friction force and shear strength between these inner walls has been estimated experimentally by two groups. Yu *et al* [9] attached a MWCN to two tips through electric discharges and then proceeded to apply a tensile load until the outer shell of the MWCN broke. Using atomic force and scanning electron microscopy, the interaction force between the walls as a function of the contact length between the outer and the inner nanotubes was measured. Two systems were studied, one 2.2 $\mu$m in length with outer diameter of 30 nm and the second 7.5 $\mu$m in length and outer diameter of 36 nm. Analysing the forces acting in this system, Yu *et al* [9] estimated that the dynamic and static shear strength were very low and equal; for the smaller system it was 0.30 MPa, while for the larger system it was 0.08 MPa. The difference between these two values was attributed to different interlayer spacing between the neighbouring shells and the degree of commensurability in the studied systems. Cumings and Zetl [8] performed a similar experiment, where one end of a MWCN was attached to a surface, while the other end was opened through a chemical reaction. The inner shell of the MWCN was attached to a tip through an electrical discharge. The inner shell was then pulled out, released from the tip through another discharge, and the nanotube retracted by itself over a period of less than 1 ns. The exact time could not be quantified due to the physical limitations. But the experiment was observed using transmission electron microscopy. Based on this upper limit for the retraction time and estimating the van der Waals forces, they estimated that the static shear strength should be less than 0.66 MPa, while the dynamic shear strength should be less than 0.43 MPa.

Simulations [22, 35–42] and theoretical studies [2, 5, 11] have predicted interesting mechanical and electromechanical applications for MWCNs. Applications as rotational molecular nanobearings have been proposed by Merkle [2], Tuzun *et al* [35] and Zhang *et al* [36]. They found that the potential energy of the nanobearing is periodic and a function of the rotational position; if the indices of the walls are chosen to have short periods for the potential energy, then the nanobearing will rotate without difficulty. The performance of these nanobearings will depend on the temperature, velocity, the size of the system, and the number of vibrational motions present in the walls [37]. Modifying this system to have electrical charges in the inner nanotube, Tuzun *et al* [35] proposed that these nanobearings could work as rotational molecular motors when two oscillating laser fields are applied to the system. From their simulation results, they obtained stable rotational motion at speeds up to about $10^{12}$ Hz. Forro [5] proposed that by modifying the inner shell to have charges, an electron current will produce a separation of the inner shell due to the Faraday cage effect; when the system is released of electron current, van der Waals interactions will restore the system to its original position. Taking into account these two effects, this system is proposed to work as an electromechanical nanoswitch. Xia and Curtin [38] simulated the pullout and friction forces of DWCNs attached to a surface and they found that end effects and defects on the DWCNs structures dominated these forces.

The last application of DWCN's that we consider was proposed by Zheng and co-workers [11, 41], and is the object of study in this work. They proposed that if both ends of the outer nanotube are eliminated, and the inner shells are pulled apart from the outer nanotube to a distance where there is still some contact area, then the nanotube will retract and will cross the outer nanotube starting a process of oscillation which will stop after some period of time. Based on estimations for the van der Waals interactions between the shells of the nanotubes, they predicted that the oscillations would show frequencies on the gigahertz scale. Guo *et al* [39] and Legoas *et al* [40] studied these oscillations at constant energy and found that the oscillations under these conditions are in the gigahertz range and that the frictional forces have the same order of magnitude as in the experiments [8]. In a preliminary account of the simulations described in this paper [42], we reported molecular dynamics simulations of oscillations in a variety of DWCNs at constant temperature. In this paper, we report these and additional findings in detail (including the development of a mathematical model to describe the simulation results). The key methodological difference between our work and that of Guo *et al* [39] and Legoas *et al* [40] is that our simulations are conducted at constant temperature. Constant energy

simulations correspond to simulations in a vacuum, where there is no avenue for heat dissipation to the environment; constant temperature implies that the nanotubes are in contact with a heat sink, and we anticipate that in any actual application of sliding nanotubes as oscillators that the nanotubes will be attached to a surface which can act as a heat sink. A realization of oscillatory nanotubes in practice will likely lie somewhere between the constant energy situation and the constant temperature one, since the DWCN will need to be attached to some surface, but depending on the thermal conductivity of the surface and the attachment area, the heat flow to the surface is likely not to be fast enough to maintain the nanotube at constant temperature. Based on our own explorations involving simulations at constant energy and at constant temperature, the oscillatory behaviour of DWCNs in these two situations is qualitatively similar but differs in quantitative details. Detailed comparisons between these two situations will be the subject of a future study; in this paper, we focus on the results from our constant temperature studies. We proceed as follows, in section 2 we describe the potential model used and in section 3 give details of the simulations performed. In section 4 we present the results and conclude in section 5.

## 2. Potential model

The potential model employed for the carbon nanotubes was developed by Guo *et al* [43]. This model consists of bond stretching (Morse potential), angle bending, coupled bond stretching–angle bending, twofold torsions for the intramolecular interactions, and Lennard-Jones intermolecular interactions between the carbon atoms that form the nanotubes. The model was fitted for $sp^2$ carbon centres using experimental lattice parameters, elastic constants and phonon frequencies for graphite and has been used to predict the packing structures of fullerenes $C_{60}$ and $C_{70}$. It has also been used to predict the heat of sublimation for these molecules in excellent agreement with experimental results [44]. Other studies have used this model to predict uniaxial-strain behaviour, packing structure, lattice parameters, vibrational modes and frequencies for bulk and insulated carbon nanotubes [45], and doped carbon nanotubes with potassium atoms [46]. This potential model was also used by Tuzun *et al* [47] to simulate the flow of fluids inside carbon nanotubes.

In the Guo *et al* [43] potential, the intramolecular interactions are given by the following equations where $E_{\mathrm{INT2}}$, $E_{\mathrm{INT3}}$,$E_{\mathrm{INT2-3}}$ and $E_{\mathrm{INT4}}$ are the 2-, 3-, coupled 2 and 3-, and 4-body interactions, respectively:

$$E_{\mathrm{INT2}}(r_{ij}) = D_2[1 - \exp(-\alpha(r_{ij} - r_e))]^2 \tag{1}$$

$$E_{\mathrm{INT3}}(\theta) = \tfrac{1}{2}D_3(\cos\theta - \cos\theta_e)^2 \tag{2}$$

$$\begin{aligned} E_{\mathrm{INT2-3}}(\theta) = {} & D_{2-3,1}(r_A - r_e)(\cos\theta - \cos\theta_e) \\ & - D_{2-3,2}(r_C - r_e)(\cos\theta - \cos\theta_e) \\ & - D_{2-3,3}(r_A - r_e)(r_C - r_e) \end{aligned} \tag{3}$$

$$E_{\mathrm{INT4}}(\phi) = D_4[1 - \cos(2\phi)] \tag{4}$$

where $r_{ij}$ is the distance between sites $i$ and $j$, $\theta$ is the angle formed by the contiguous bonds $r_A$ and $r_C$ and $\phi$ is the dihedral angle. The parameters for equations (1)–(4) are (where $k_{\mathrm{B}}$ is Boltzmann's constant): $D_2/k_{\mathrm{B}} = 3283.88$ K, $\alpha = 2.186\,76$ Å$^{-1}$, $r_e = 1.418$ Å, $D_3/k_{\mathrm{B}} = 98\,706.59$ K, $\theta_e = 120.00°$, $D_{2-3,1}/k_{\mathrm{B}} = D_{2-3,2}/k_{\mathrm{B}} = -36\,441.87$ K Å$^{-1}$, $D_{2-3,3}/k_{\mathrm{B}} = 34\,222.44$ K Å$^{-2}$, and $D_4/k_{\mathrm{B}} = 5354.81$ K.

Intermolecular interactions include Lennard-Jones interactions between carbon atoms of different molecules:

$$E_{\mathrm{LJ}}(r_{ij}) = 4\varepsilon\left[\left(\frac{\sigma}{r_{ij}}\right)^{12} - \left(\frac{\sigma}{r_{ij}}\right)^{6}\right] \tag{5}$$

where $\varepsilon/k_{\mathrm{B}} = 34.83$ K and $\sigma = 3.4$ Å.

Carbon nanotubes are large molecules with hundreds of atoms, each of which can participate in up to three bond-stretch, nine angle-bend and 26 torsional interactions. However, the periodicity of the unit cells that form the nanotube helps define and calculate these interactions in a computationally efficient manor in a simulation program [48].

## 3. Methodology and simulations details

The algorithm employed to integrate the equations of motion was the reversible reference system propagator algorithm (r-RESPA) developed by Tuckerman *et al* [49] with a Nosé thermostat [50, 51]. In this algorithm, fast (intramolecular forces) and slow motions (intermolecular interactions) are integrated over different timescales. The system is coupled to a Nosé bath with an appropriated coupling variable that produces small fluctuations when the temperature of the bath is readjusted. This algorithm has been tested for macromolecules (proteins and fullerenes) [52, 53] and compared to standard Verlet algorithms it has been shown to speed up the computation time between 4–5, and 20–40 times for systems with, and without, electrostatic interactions, respectively. The time-steps for slow and fast motion employed in this work were 2.21 and 0.221 fs, respectively. The motivation for applying a thermostat, as outlined in the introduction, is that nano-mechanical systems are generally studied experimentally attached to large surfaces or other structures that are thermally equilibrated [8, 9]. These large surfaces or structures dissipate the kinetic energy produced by friction forces during a mechanical event involving the nano-mechanical system thus keeping the whole system thermally equilibrated [38]. For this reason, the simulated system was thermostatted but only in the radial direction. This is simply for convenience, since it does not require us to remove the translational motion in the axial direction that does not contribute to the temperature of the system.

In this work, molecular simulations of the oscillatory behaviour of DWCNs proposed by Zheng and Jiang [11] were performed using molecular dynamics in the canonical ensemble. Before the oscillatory phenomena can occur, the DWCN systems are pulled apart in order to have a small area of contact; retraction occurs followed by the oscillations. Simulations were carried out in three steps, initial equilibration with no external force, followed by a period with external force applied until separation occurs, and then release of the external force leading to the oscillatory behaviour. The initial configurations were equilibrated for a period of 22 ps. After that, an external force was applied to the inner nanotube, and a force with the same magnitude but opposite sign was applied to the outer nanotube. The applied external force was

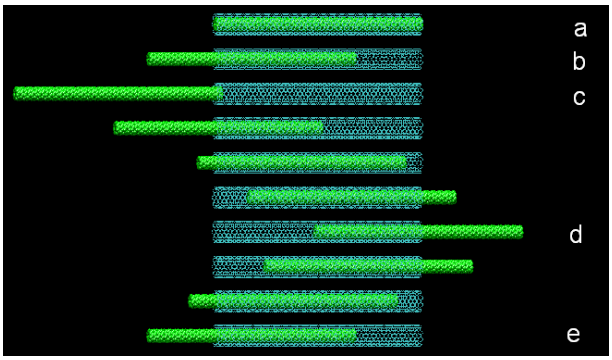


**Figure 1.** Snapshots of the separation induced through an external force and the damped oscillatory behaviour after the system is released from the external force. The system plotted corresponds to the (7, 0)@(9, 9) structure with length of 12.21 nm. The labelled steps are (a) force applied to the initial equilibrated system, (b) releasing the system from the external force, (c) first minima of separation in the first end, (d) first maxima in the second end and (e) second minima in the first end.
M Multimedia of this figure is available from stacks.iop.org/Nano/16/186

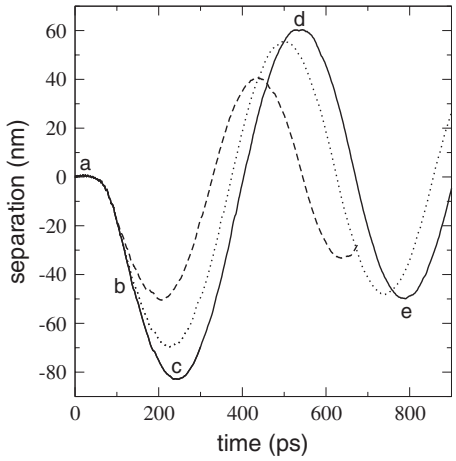


**Figure 2.** Separation of centres of mass as a function of time for the (7, 0)@(9, 9) structure with length of 98.24 nm at 298.15 K. The three curves correspond to the system exposed to longer periods of external force. Points (a) through (e) correspond to the snapshot in figure 1.

a function of the simulation time and was built by mixing step and hyperbolic tangent functions [48]. The advantage of using this profile is that there are short periods when the force is incremented followed by periods where the force remains constant; this allows the system to relax before a new increment in the magnitude of the force occurs. Before using this profile of the external force, we used constant increments of the external force. However, this approach produced very low separations or complete separation of the two nanotubes, since the low friction forces in these systems makes it difficult to control the distance of separation. A sketch of the phenomena simulated is shown in figure 1, where at step (a) two external forces with opposite directions are applied to an equilibrated DWCN. Once the magnitude of the force is high enough, the system starts to separate and before the system separates completely the external force is eliminated (b). Due to the impulse of the external applied force and the low friction forces between the walls, the nanotube continues separating until it reaches a separation with some minimal contact area (c). The magnitude of the contact area is clearly a function of when the external force is set to zero. Hence, the time (b) where the external force is eliminated was tested by trial and error until the separation at time (c) corresponded to a contact area of a few ångströms. After this event, the inner nanotube retracts by itself due to the attractive van der Waals interactions and after reaching a zero separation, the nanotube continues its movement until it reaches a maximum extension in the opposite direction (d). It then continues oscillating until finally coming to rest at the equilibrium position (zero separation) again.

The effect of the magnitude of the initial applied external force is shown in figure 2 for the (7, 0)@(9, 9) structure and a length of 98.24 nm. In this figure the separations in the axial direction between the centres of mass of both nanotubes are plotted as a function of time. After 50 ps of increments in the magnitude of the external force, the system starts to separate and at point (b) (∼125 ps) the system is released of the external force. Even though the system has a separation of only ∼32 nm at this point, the system continues separating until it reaches a maximum separation of ∼83 nm at ∼243 ps, corresponding to a minimal overlap between inner and outer nanotubes. Points (d) and (e) correspond to the similar events marked in the sketch of figure 1. The dotted and dashed lines in the figure correspond to the second and third 'experiments' where the magnitude of the external force was smaller. For the second 'experiment' even though the initial separation at point (b) is ∼24 nm, the system reached a maximum at ∼70 nm, for the third 'experiment' the corresponding separations were ∼11 and ∼50 nm.

## 4. Results

The procedure described in the last section was applied to the incommensurate (7, 0)@(9, 9) structure at 298.15 K. Five systems with axial lengths of 12.21, 24.56, 36.92, 49.27 and 98.24 nm were studied; for these systems, the inner and outer shell had the same axial lengths. Additionally simulations were performed keeping the inner length at 12.21 nm and using axial lengths for the outer nanotube with −30% to +40% increments with respect to the inner nanotube axial length.

### *4.1. The incommensurate system (7, 0)@(9, 9)*

The incommensurate system with (7, 0)@(9, 9) structure was simulated for the inner and outer nanotubes of equal axial lengths at 298.15 K. For this structure, the carbons in the outer shell are located in a cylinder with diameter of 1.22 nm (defined as the distance between the centres of carbon atoms on opposite sides of a cross section of the nanotube) and the intershell separation between the inner and outer cylinders is 0.34 nm. Five systems were simulated with axial lengths of 12.21, 24.56, 36.92, 49.27 and 98.24 nm. These systems contained between 2600 and 21 000 carbon atoms. Results of the separation between the centres of mass as a function of time are shown in figure 3; this plot shows the simulation results starting from the point where the system reached the first minimum or point (c) in figure 2. This facilitates comparison between the different simulations. Simulations

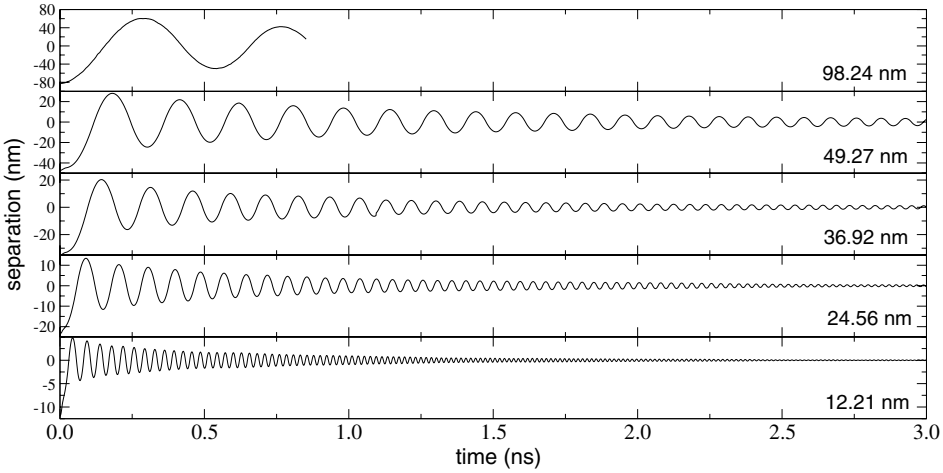


**Figure 3.** Separation of the centres of mass as a function of time for the (7, 0)@(9, 9) structure with lengths from 12.21 to 98.24 nm at 298.15 K. The initial separation corresponds to a contact length of 0.3 nm.

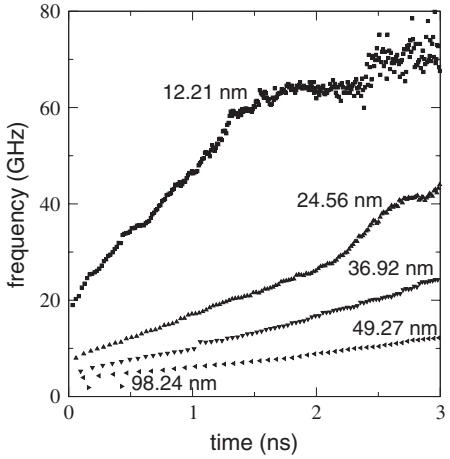


**Figure 4.** Frequency of the damped oscillations as a function of time for the (7, 0)@(9, 9) structure with axial lengths from 12.21 to 98.24 nm at 298.15 K.

were performed for 3 ns and over this period of time only the smallest system ceased oscillations almost completely (at ∼2.5 ns). For the largest system only 0.85 ns were simulated because of limitations on computational resources available to simulate a 21 000-carbon-atom system. In this shorter time period, corresponding to almost two complete oscillations, the 98.24 nm system exhibited the same qualitative behaviour as the smaller systems. The first oscillation in all systems seemed to have different dynamics than the later oscillations, because the relation between the minimum and maximum separations in that oscillation has a significantly larger ratio than subsequent oscillations.

The frequency of each oscillation was calculated for all systems and the profile of these frequencies of oscillation are plotted in figure 4 as a function of time. All systems showed frequencies of the order of gigahertz, consistent with prior theoretical work [11, 41]. Frequencies of this magnitude have also been reported for other nanoscale systems, such as the oscillatory attraction–repulsion of two nanoparticles of long hydrocarbon molecules in vacuum [54]. In general terms, the average value of the frequency in each profile decreases with the axial length of the system. For the smallest nanotube, frequencies started at ∼19 GHz, and increased almost linearly for ∼1.65 ns to a value of ∼63 GHz with a slope of ∼27 GHz ps$^{-1}$. After this point, the frequencies remained almost constant for the remainder of the simulation. After the damped oscillations essentially ceased (∼2.5 ns), the natural modes in the axial vibration of both nanotubes make small oscillations with high frequencies having an average value ∼75 GHz but with large fluctuations (∼8 GHz). Hence, the system has come to equilibrium and these oscillations are thermal in nature. For the system with axial lengths of 24.56, 36.92 and 49.27 nm, there is also a period of time where the simulations increased linearly with slopes of 9.68, 6.43 and 2.91 GHz ps$^{-1}$, respectively. From these profiles it is obvious that, during the course of the simulations, the systems with axial lengths of 24.56 nm and up did not reach an equilibrated configuration where the oscillations are thermal in nature. We were only able to run the largest system for a period corresponding to two oscillations, so the dependence of frequencies on time cannot be extracted over such a short trajectory. In order to perform a more rigorous comparison between the frequencies and the axial length of the system, the initial frequency is plotted against the axial length in figure 5. The open circles represent the simulation results for the frequency $f$ and the red curve represents the best fitting using a function proportional to the inverse of the axial length:

$$f\,(\mathrm{GHz}) = \frac{197.903\ (\mathrm{GHz\ nm})}{\mathrm{length\ (nm)}}. \tag{6}$$

This dependence on nanotube length is in agreement with theoretical predictions of Zheng and Jiang [11], where they estimated that the frequency of these oscillations as

$$f = \frac{\beta}{4}\sqrt{\frac{c_1\Pi}{L_c\Delta}} \tag{7}$$

with $\beta = \sqrt{1-\delta}/(1-\delta/2)$, where $\delta = |L_o - L_c|/2\Delta$ is the relative length mismatch, $\Delta$ is the initial extension, $L_o$ and $L_c$ are the length of the inner and outer shells, respectively, $c_1$ is a variable that depends on the number of shells and their intershell separation, and $\Pi$ is an average value for the van der Waals interactions that depends only on the number of shells

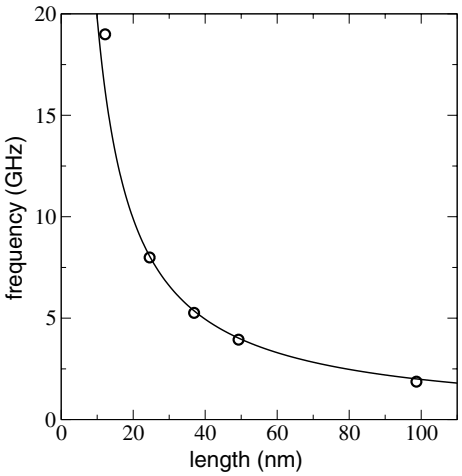


**Figure 5.** Frequency of the initial oscillation as a function of the axial length of the nanotubes for the (7, 0)@(9, 9) structure. The curve is the best-fitted curve to the inverse of the length.

in the core. For our simulations, the inner and outer shells had the same length ($\beta = 1$), and the frequency will depend only on the initial axial separation and the inner shell lengths, which for our case had almost the same value ($\Delta \approx L_c$), therefore the frequency will be proportional to the inverse of the axial length, as found in the simulation results.

### *4.2. Mechanical model with constant effective forces*

In order to understand the forces that contribute significantly to this damped oscillatory behaviour, a mechanical model was developed. In figure 6 two oscillations for the nanotube with axial length of 24.56 nm are shown in the top of the figure from 0.05 to 0.28 ns. The velocities of these separations were calculated as the numerical derivatives and are also shown in figure 6. The axial and normal forces acting on the inner nanotube were computed during the simulation and are plotted in the bottom of figure 6. The velocities show small fluctuations close to the zero separations, reflecting the behaviour of the axial force, which abruptly changes in sign at those points. From the velocity profiles we can conclude that the slopes are constant, therefore the acceleration should be constant and will depend only on the sign of the separation, hence a constant effective force should describe this behaviour. Examining the profiles of the axial force, we can see that the inner nanotube feels almost constant axial forces when the inner nanotube is entering or leaving the outer nanotube and changes sign when the nanotube is passing through zero separation. The normal forces acting over the inner nanotube are high compared to the axial forces (∼5:1), but the actual forces that dictate how the system behaves will be a fraction of these forces.

If we divide one oscillation into four regions as shown by the black curve in figure 7, then we can see that we have equivalent regions when the inner nanotube is entering the outer nanotube from one or the other end, and when the inner nanotube is leaving. In region I of figure 7, when the inner nanotube is entering from one end we assume that the tube experiences a constant force $F_I$ that opposes the motion (see

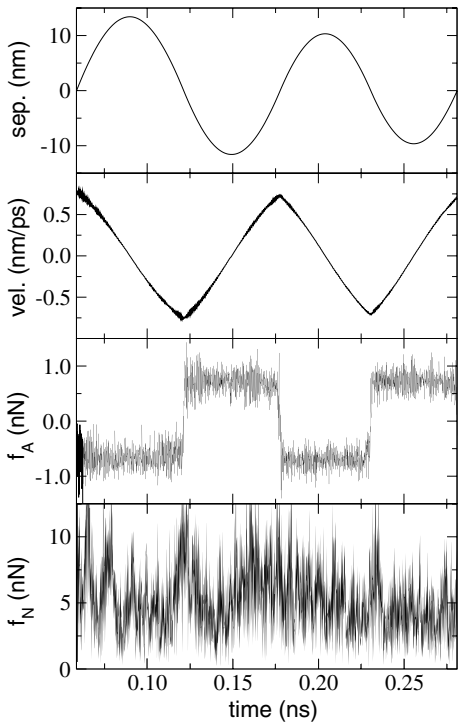


**Figure 6.** Two oscillations of the separation of the centres of mass for the system with length of 24.56 nm. Velocities are the numerical derivative of the separation $f_A$ and $f_N$ are the axial and normal forces, respectively, acting over the inner nanotube during the simulation.

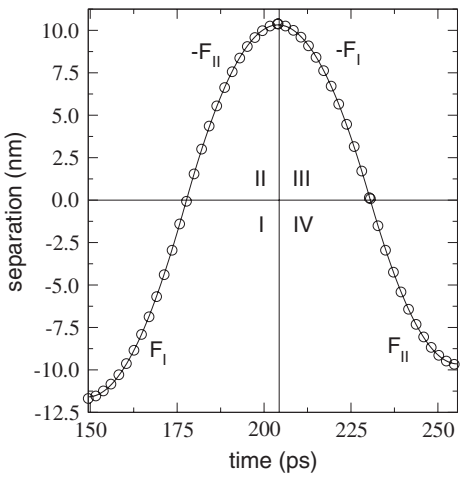


**Figure 7.** Division of the oscillation in four sections with different constant effective forces. Black circles represent the fittings to the mechanical model.

figure 6). We can solve the differential equation,

$$F_I = m_n \frac{d^2 z}{dt^2} \tag{8}$$

with boundary conditions:

$$\frac{dz}{dt}(t = 0) = 0$$
$$z(0) = z_0 \tag{9}$$

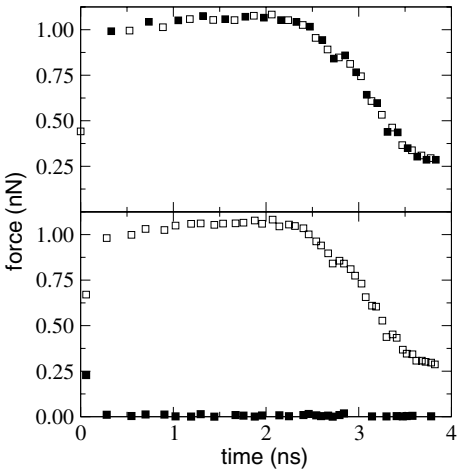


**Figure 8.** Values of the constant effective forces $F_{\mathrm{I}}$ (open squares) and $F_{\mathrm{II}}$ (filled squares) for the (7, 0)@(9, 9) structure with length of 24.56 nm (top). Contributions $F_{\mathrm{VDW}}$ (open squares) and $F_{\mathrm{FR}}$ (filled squares) to the constant effective forces (bottom).

to produce:

$$z = z_0 + \frac{F_{\mathrm{I}}}{2m_{\mathrm{n}}}t^2 \tag{10}$$

where $m_{\mathrm{n}}$ is the mass of the inner nanotube, $z$ is the separation of the inner nanotube centre of mass from the outer nanotube centre of mass and $z_0$ is the initial separation. For region III, the same equation applies but the effective force has an opposite sign. For region II, a similar procedure yields:

$$z = v_0 t - \frac{F_{\mathrm{II}}}{2m_{\mathrm{n}}}t^2 \tag{11}$$

where $v_0$ is the initial velocity at $z = 0$ in region II. The profile in figure 7 was fitted to these expressions, and is shown with black circles. Each oscillation of the system with axial length of 24.56 nm was fitted using equations (10) and (11) and the equivalent equations for regions III and IV. Results of the absolute fitted values for the effective forces ($F_{\mathrm{I}}$ and $F_{\mathrm{II}}$) are shown in the top of figure 8. For this system, the effective forces have almost the same value and remain constant from the second or third oscillation to ∼2.5 ns. In this case the mechanical model proposed using a constant value for these effective forces will be valid for the same period of time. If we divide these forces into a contribution due to the van der Waals attractions and a force that opposes the movement of the nanotube ('friction force'), which will have an opposite sign to the direction of the velocity of the inner nanotube, then we can express $F_{\mathrm{I}}$ and $F_{\mathrm{II}}$ as:

$$\begin{aligned}
&\text{I: } F_{\mathrm{I}} = F_{\mathrm{VDW}} - F_{\mathrm{FR}}, && \mathrm{d}z/\mathrm{d}t > 0, \quad z < 0\\
&\text{II: } F_{\mathrm{II}} = -F_{\mathrm{VDW}} - F_{\mathrm{FR}}, && \mathrm{d}z/\mathrm{d}t > 0, \quad z > 0\\
&\text{III: } F_{\mathrm{III}} = -F_{\mathrm{VDW}} + F_{\mathrm{FR}} = -F_{\mathrm{I}}, && \mathrm{d}z/\mathrm{d}t < 0, \quad z > 0\\
&\text{IV: } F_{\mathrm{IV}} = F_{\mathrm{VDW}} + F_{\mathrm{FR}} = -F_{\mathrm{II}}, && \mathrm{d}z/\mathrm{d}t < 0, \quad z < 0.
\end{aligned} \tag{12}$$

Using equations (12) to fit every region of each oscillation, we calculated $F_{\mathrm{VDW}}$ and $F_{\mathrm{FR}}$ as a function of the simulation time. The results are plotted in the bottom of figure 8. From these plots we can see that the so-called 'friction force' is very low compared to the van der Waals attractions and that there are other contributions that make the effective forces decrease at the beginning and after 2.5 ns when the amplitude of the oscillations decreases considerably.

Using an averaged value of $F_{\mathrm{VDW}}$ and $F_{\mathrm{FR}}$ from the bottom of figure 8 in the period of 0.2–2.5 ns as an initial estimation, then these values were optimized to reproduce the points corresponding to a zero separation for the system with an axial length of 24.56 nm. This procedure produced values of 1.05 and 0.024 nN for the $F_{\mathrm{VDW}}$ and $F_{\mathrm{FR}}$, respectively. These parameters are highly coupled and changes of either one by as little as 1% can modify the behaviour. With these parameters, the damped oscillations were reproduced for the studied systems using equations (10) and (11). The results of these predictions from the mechanical model for the separation between the centres of mass for the systems with axial lengths of 12.21 and 49.27 nm are shown in figure 9 by the red lines. For the nanotube with an axial length of 12.21 nm, the mechanical model reproduces the profile of the simulations up to ∼0.8 ns well, and is observed to oscillate with the same amplitude. For the system with 24.56 nm (not shown), the model predictions reproduce the behaviour up to ∼1.75 ns; for the systems with 36.92 (not shown) and 49.27 nm the predictions agree well up to ∼2.6 ns, however the model misses two oscillations at ∼1.5 and ∼2.0 ns for the system with 36.92 nm, and one oscillation at ∼2.2 ns for the system with 49.27 nm. The regions of mismatch between the simulations and the model for the 36.92 and 49.27 nm systems suggest that the frequency of motion predicted by the model is slightly off from the measured value. This is not surprising with such a simple model.

### *4.3. Mechanical model with constant effective forces depending on the initial conditions*

In the early stages of the damped oscillation, deformations in the cylinder of both the inner and outer nanotubes are observed. The reader can observe these deformations in the visualization provided for the system with an axial length of 12.21 nm in the multimedia file available at stacks.iop.org/Nano/16/186. These deformations make it more difficult for the inner nanotube to enter into the outer nanotube and therefore these forces have an opposite sign to the van der Waals interactions and will reduce the absolute value of the effective force. On the other hand, when the nanotube is close to a zero separation, both ends of the inner nanotube are close to their corresponding ends in the outer nanotube and the magnitude of the effective force does not change from positive to negative instantaneously, but over a short period of time (corresponding approximately to the time required for the inner nanotube to move a distance of the order of one carbon diameter). For this reason after 2.5 ns when the oscillations almost cease, the magnitude of the effective force in figure 8 also starts to decrease. We were not able to produce a profile with the real instantaneous force as a function of the separation that produces a better description of the damped oscillations than the constant effective forces model. Given the shortcomings of the first model a second model was identified. In the second mechanical model described in this section, we use constant effective forces along each region (I, II, III, IV) as in the previous model, but the value of the constant effective forces depends on the initial separation for regions I and III, and on the initial velocity for regions II and IV.

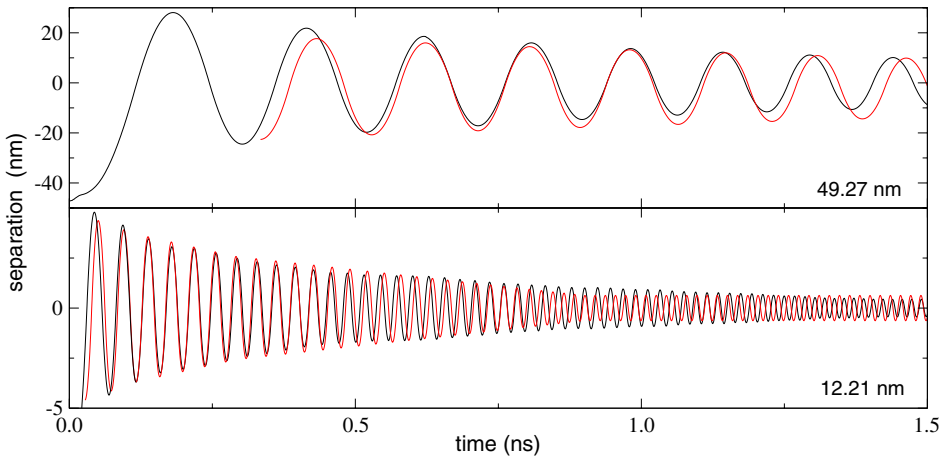


**Figure 9.** Damped oscillations from simulations (black curve) and predictions (red curve) of the mechanical model with constant effective forces for the (7, 0)@(9, 9) structure with axial lengths of 12.21 and 49.27 nm at 298.15 K.

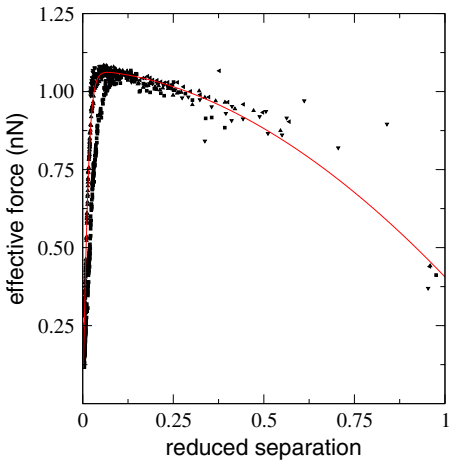


**Figure 10.** Effective forces (regions I, III) as a function of the initial reduced separation for the (7, 0)@(9, 9) structure with axial lengths from 12.21 to 98.24 nm. Symbols are the same as figure 4. The continuous curve represents the plotting of equation (13) with optimized parameters to reproduce the behaviour of the 24.56 nm system.

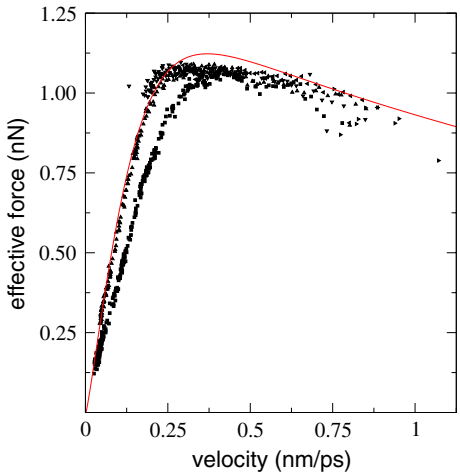


**Figure 11.** Effective forces (II, IV) as a function of the initial velocity for the (7, 0)@(9, 9) structure with axial lengths from 12.21 to 98.24 nm. Symbols are the same as figure 4. The continuous curve represents the plotting of equation (14) with optimized parameters to reproduce the behaviour of the 24.56 nm system.

In order to build a second mechanical model which takes into account the deformation forces for longer separations and a better description of the effective forces close to zero separation, the oscillations of all systems were fitted to equations (10) and (11). The fitted values for the effective forces for regions I and III for all systems studied are plotted in figure 10 as a function of the initial reduced separations $z_r$. The separations were reduced by the axial length of each system. The initial reduced separations, plotted in figure 10, are the separations at the beginning of regions I and III, or in other words, they are the maximum and minimum separations reached in those regions, respectively. Only the smallest system has a different behaviour for initial reduced separations up to 0.15. The points for the rest of the systems seem to lie on the same master profile. In this master profile at the beginning there is a linear increment of the absolute effective force with the initial reduced separation up to a separation of ∼0.05. At this point the effective forces have a maximum, and from this point to separations close to 1.0, the effective forces decrease with the reduced separation. From reduced separations of ∼0.3 and up, the force shows some dispersion but follows the general tendency to decrease with the reduced separation. For regions II and IV, the fitted values to equation (11) for the absolute effective forces are plotted in figure 11 as a function of the initial velocity. Here it is clear that the smallest system behaves differently from the rest of the systems. These profiles show the same tendency as those for regions I and III, i.e. an initial linear increase at low initial velocities, reaching a maximum from which the absolute effective forces decrease with the initial velocity.

Using only effective forces data that correspond to the systems with axial lengths from 24.56 to 98.24 nm, two functions were fitted, one depending on the initial reduced separation (regions I and III), and one for the forces depending on the initial velocity (regions II and IV). Those functions are:

$$F_{\mathrm{I}} = A_0 \tanh\left(\frac{z_{\mathrm{r}}}{A_1}\right) - A_2(z_{\mathrm{r}})^{A_3} \qquad (13)$$

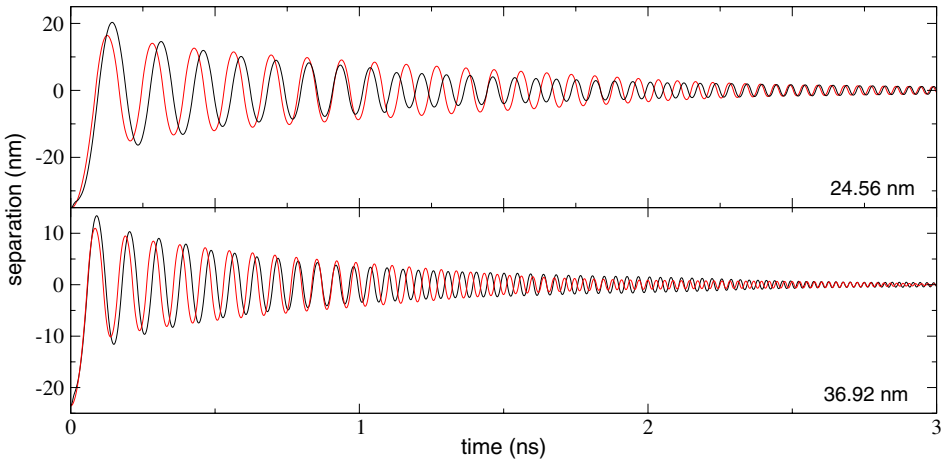


**Figure 12.** Damped oscillations from simulations (black curve) and predictions (red curve) of the mechanical model with effective forces dependent of the initial conditions. The (7, 0)@(9, 9) structures has axial lengths of 24.56 and 36.92 nm at 298.15 K.

$$F_{\mathrm{II}} = B_0 \tanh\left(\frac{v_0}{B_1}\right) - B_2(v_0)^{B_3}. \qquad (14)$$

These functions were first fitted to the mentioned points and then optimized to reproduce the zeros of the separation profile for the system with axial length of 24.56 nm. The optimized parameters were: $A_0 = 1.014\,281$ nN, $A_1 = 0.037\,059$, $A_2 = 0.743\,32$ nN, $A_3 = 1.4107$, $B_0 = 1.6358$ nN, $B_1 = 0.217\,01$ nm ps$^{-1}$, $B_2 = 0.878\,21$ nN nm$^{-0.515\,00}$ ps$^{0.515\,00}$ and $B_3 = 0.515\,00$. The optimized functions are shown as black curves in figures 10 and 11 for regions I, III and II, IV, respectively. The functions fit the values for initial reduced separations up to 0.25 and ∼0.30 nm ps$^{-1}$ for the initial velocities very well.

Calculating the absolute effective forces using functions (13) and (14), we can reproduce the whole simulation process as shown in figure 12 for the systems with axial lengths of 24.56 and 36.92 nm. The predicted behaviour of the mechanical model dependent on the initial conditions is shown by the red curves and the simulation results by the black curves. The best agreement between the damped oscillations of the simulations and the predicted oscillations by the mechanical model are for times up to 1 ns in the system with axial length of 24.56 nm, while for times after 2.25 ns the best predicted behaviour is for the system with axial length of 36.92 nm. For the system with axial length of 24.56 nm, the poor results obtained using this model are probably due to the small disagreement between the optimized curve and the fitted values of $F_{\mathrm{II}}$ for initial velocities between 0.3 and 0.6 in figure 11.

Using the maximum for the effective force in figure 10 as the dynamic strength force, which is the same for nanotubes with axial length of 24.56 nm and up, we can predict the dynamic strength for these systems. Defining the interfacial area as $2\pi RL_{\mathrm{c}}$, where $R$ is the average of the inner and outer nanotubes radii, then we can calculate the dynamic strength; results of these calculations are shown in figure 13 as a continuous curve for systems with axial lengths from 350 to 7000 nm. Experimental estimations for these strengths are shown in black circles for the system of Cumings and Zetl [8] with 330 nm of axial length (the actual length of the system was not reported, the only length reported was the extrusion length, which is assumed to be close to the axial length of the system)

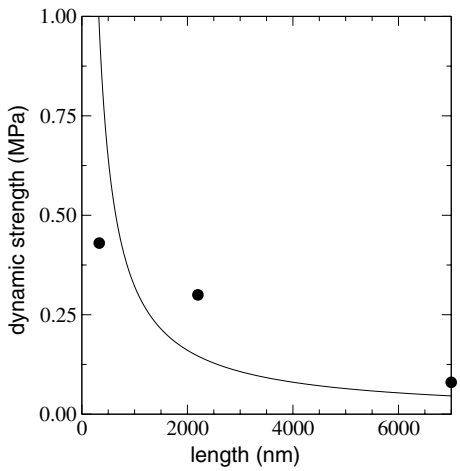


**Figure 13.** Dynamic strength as a function of the axial length for the (7, 0)@(9, 9) structure at 298.15 K. Black circles represent experimental values at 330 nm [8], 2200 and 7000 nm [9].

but the diameter was not reported. The results of Yu *et al* [9] are also shown at 2200 nm and 7000 nm for system with outer diameters of 30 and 36 nm, respectively. The predicted dynamic strength is proportional to the inverse of the axial length, and the agreement with the largest experimental system is particularly good (absolute difference of ∼0.04 MPa). The predicted curve is only for incommensurate nanotubes with an outer diameter of 1.22 nm. For systems with larger outer diameters, there are likely to be four main effects: the increase in the van der Waals interactions due to the larger number of carbon atoms forming the unit cell will increase the shear strength; the larger area will decrease the strength; for wider systems the deformations will be larger and will decrease the dynamic strength. Finally, the fourth effect will be the chiral indices of each nanotube. How this affects the system is ill-defined [22, 23].

Using this mechanical model, the time needed to reduce the oscillations to amplitude of less than 4 nm was calculated for systems with axial length up to 1000 nm and the results are reported as black circles in the top right plot of figure 14. The value of 4 nm was chosen because for a system of 1000 nm

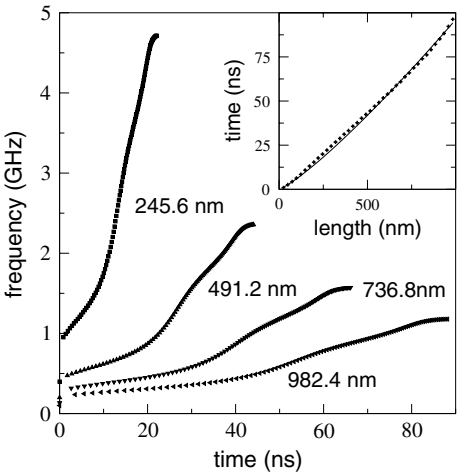


**Figure 14.** Predicted frequency profiles as a function of time for the (7, 0)@(9, 9) structure with axial lengths from 245.6 to 982.4 nm at 298.15 K. Required time to decrease the amplitude of the oscillations to 4 nm as function of the length (inside plot). The continuous curve represents the fitted function to a power of the axial length.

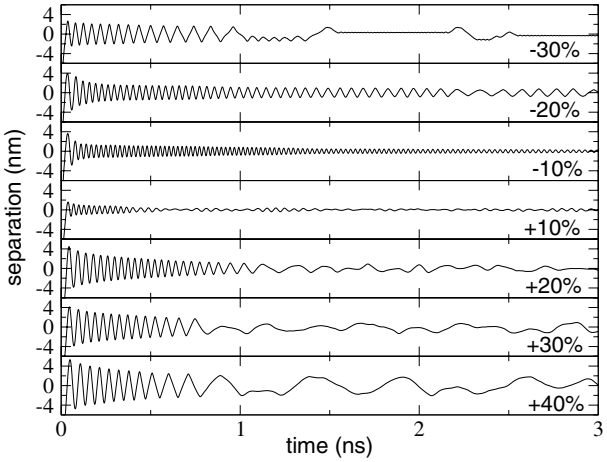


**Figure 15.** Separation of the centres of mass as a function of time for the (7, 0)@(9, 9) structure with inner nanotube axial length of 12.21 nm and outer nanotube axial length from −30% to +40% of the inner axial length at 298.15 K.

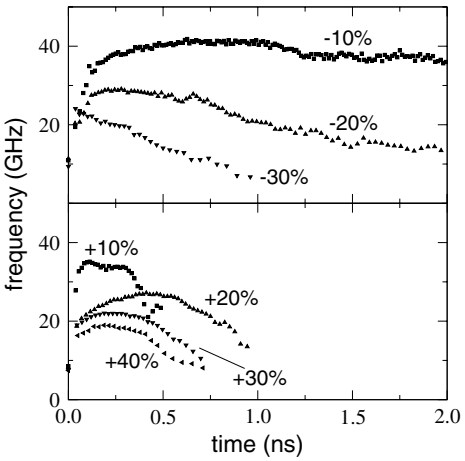


**Figure 16.** Frequency of the damped oscillations as a function of time for the (7, 0)@(9, 9) structure with inner nanotube axial length of 12.21 nm and outer nanotube axial length from −30% to +40% of the inner axial length at 298.15 K.

the normal axial modes of vibration will produce vibrations of this magnitude. The continuous curve represents the best fit to a power function, and is given by:

$$\text{time (ns)} = (0.024\,176\ \text{ns nm}^{-1.2})(\text{length (nm)})^{1.2}. \quad (15)$$

Predictions of the profiles for the frequencies as function of the time were produced for four structures between 245 and 982 nm, and the results are shown in figure 14. The profiles were stopped when the amplitude of the oscillations were less than 4 nm. Even though all systems reached frequencies of oscillation above 1 GHz at the beginning of the process, only the 245.6 nm system exhibits gigahertz frequencies. As in the previous simulations of shorter systems, the frequencies decrease with the axial length.

### *4.4. The incommensurate system (7, 0)@(9, 9) with unequal axial lengths*

The effect of different axial lengths was studied using an inner nanotube with axial length of 12.21 nm and seven different systems where the axial length of the outer nanotube changed from −30% to +40% of the length of the inner tube. Results for the damped oscillation profiles are shown in figure 15. The first case depicted in figure 15 shows that by reducing the length of the outer nanotube by 10%, we obtain initially faster equilibrations, however the nanotube does not finish the damped oscillations because the centre of mass of the inner nanotube is moving between both ends of the outer nanotube. This phenomenon is clearer for the cases where the outer nanotube is 20 and 30% shorter respectively. Using larger outer nanotubes we can also obtain very fast equilibrations as in the case where the outer nanotube is 10% larger and after ∼0.5 ns the damped oscillations have almost completely ceased, but the oscillations never exceed an amplitude of 2 nm. If the axial length of the outer nanotube is increased by 20% then it takes ∼1 ns for the well-defined damped oscillations to finish, while for the systems with 30% and 40% larger outer nanotubes, it takes ∼0.75 ns to finish. Beyond these times, we observe erratic behaviour, which probably reflects large thermal fluctuations.

The frequencies of oscillation were calculated for all cases and appear in the top of figure 16 for the systems with shorter outer nanotubes and in the bottom of the figure for the systems with larger outer nanotubes. The case where both lengths are the same is used as a reference case and it is plotted in both figures for comparison. Compared to the reference case, shorter outer nanotubes have bigger frequencies at the beginning of the motion, but then reaches a maximum and starts to decrease. The rate of decrease is faster for the shortest outer nanotube. For the case where the outer nanotube is 10% larger in axial length than the inner nanotube, the frequencies are higher than the reference case, but for the other cases they are generally lower and the well-defined damped oscillations last for less than 1 ns.

The absolute effective forces were calculated for all cases and are shown in figure 17. In general we can see a movement of the force profiles to the right reflecting the differences

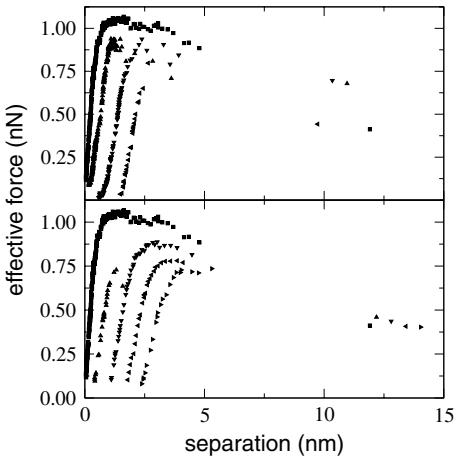


**Figure 17.** Effective forces (regions I, III) as a function of the initial separation (top) for the (7, 0)@(9, 9) structure, 298.15 K and (from left to right) even axial lengths, 10%, 20% and 30% shorter outer nanotube. Effective forces (regions I, III) as a function of the initial separation (bottom) for the (7, 0)@(9, 9) structure, 298.15 K and (from left to right) even axial lengths, 10%, 20%, 30% and 40% longer outer nanotube.

between the axial lengths of the inner and outer nanotubes. There is also a decrease in the magnitude of the absolute axial forces no matter if the outer nanotube is shorter or larger; the maximum absolute attractive force is reached when both nanotubes has the same axial length. The case with a 10% larger outer system is very interesting, because the maximum absolute effective force $F_I$ decreases by ∼25%, but for the next system (+20% larger) this force increases again by ∼17% and from there continues to decrease regularly.

## 5. Conclusions

DWCNs are nano mechanical systems that have potential applications as nanodevices to control nanofluids and as nanobearings and nanomotors. This study focused on the dynamics of the forces that are important in these systems. The damped oscillatory behaviour of the motion between the centres of mass of DWCNs was studied.

The incommensurate (7, 0)@(9, 9) structure was studied for axial lengths between 12.21 and 98.24 nm. A time of ∼2.5 ns was needed to cease the oscillation in the smaller system. The frequencies of oscillation obtained from these simulations have gigahertz magnitudes. The initial frequency of oscillation is inversely proportional to the axial length of the system in agreement with theoretical predictions. Two mechanical models were developed to understand and reproduce these damped oscillations. The first model only takes into account constant van der Waals interactions and a constant force related to the definition of the friction force. This model is only valid for approximately half of the simulated time, when these forces are constant. The second mechanical model takes into account the deformation forces that are important at long separations. The effective forces used by this model depend on the maximum and minimum separations and the velocities when the nanotube cross the zero separations in each oscillation. This model is valid for the whole oscillatory process and reproduced the simulated damped behaviour well. The profile of these effective forces showed a maximum at ∼5% of separation. Using this maximum force as the dynamic force strength, the dynamic strength was calculated and found to be inversely proportional to the length of the system. An absolute difference of 0.04 MPa with the estimated experimental result for this property was found. Predictions were produced for the time required to decrease the amplitude of the oscillations to less than 4 nm and for the profiles of the frequencies of oscillation.

The incommensurate (7, 0)@(9, 9) structure was also studied with unequal axial lengths between the inner and outer nanotubes. The axial length of the inner nanotube was kept constant, while the length of the outer nanotube was varied from −30% to +40% of the inner axial length. These systems equilibrated faster, but after equilibration the behaviour is somewhat erratic and requires further investigation. A maximum absolute effective force is reached only for the nanotubes with the same axial length, however the system where the outer nanotube is 10% larger equilibrates much more rapidly (∼0.5 ns).

In a future paper we will discuss the effects of temperature, commensurability, interlayer separation, interlayer filling, non-axial external forces and resonance on the frequencies of oscillation, dynamic shear strength and effective forces.

## Acknowledgments

This research was supported by Division of Chemical Sciences, Geosciences and Biosciences, Office of Basic Energy Sciences, US Department of Energy. Calculations were performed at the Center for Computational Sciences at Oak Ridge National Laboratory, the National Energy Research Supercomputing Center at Lawrence Berkeley Laboratory, and on the SinRG cluster at the University of Tennessee, supported by NSF grant EIA-9972889. Additionally, JLR thanks PROMEP (SEP)–México and the Universidad Michoacana de San Nicolás de Hidalgo (CIC) for the provided grants.

## References

[1] Buldum A and Lu J P 2001 *Phys. Rev.* B **63** 161403
[2] Merkle R C 1993 *Nanotechnology* **4** 86
[3] Sohlberg K, Tuzun R E, Sumpter B G and Noid D W 1997 *Nanotechnology* **8** 103
[4] McCurdy C W, Stechel E, Cummings P T, Hendrickson B and Keyes D 2002 Theory and modeling in nanoscience *Report of Workshop Department of Energy*
[5] Forro L 2000 *Science* **289** 560
[6] Drexler K E 1992 *Molecular Machinery, Manufacturing, and Computation* (New York: Wiley–Interscience)
[7] Drexler K E 1999 *Trends Biotechnol.* **17** 5
[8] Cumings J and Zettl A 2000 *Science* **289** 602
[9] Yu M-F, Yokobson B I and Ruoff R S 2000 *J. Phys. Chem.* B **104** 8764
[10] Yu M-F, Lourie O, Dyer M J, Moloni K, Kelly T F and Ruoff R S 2000 *Science* **287** 637
[11] Zheng Q and Jiang Q 2002 *Phys. Rev. Lett.* **88** 045503
[12] Iijima S 1991 *Nature* **354** 56
[13] Li Y M, Kim W, Zhang Y G, Rolandi M, Wang D W and Dai H J 2001 *J. Phys. Chem.* B **105** 11424
[14] Siegal M P, Overmyer D L and Provencio P P 2002 *Appl. Phys. Lett.* **80** 2171
[15] Suh J S and Lee J S 1999 *Appl. Phys. Lett.* **75** 2047

[16] Dresselhaus M S, Dresselhaus G and Avouris P H 2001 *Carbon Nanotubes: Synthesis, Structure, Properties, and Applications* (Berlin: Springer)
[17] Wildoer J W G, Venema L C, Rinzler A G and Smalley R E 1998 *Nature* **391** 59
[18] Odom T W, Huang J-L, Kim P and Lieber C M 1998 *Nature* **391** 62
[19] Kociak M, Suenaga K, Hirarhara K, Saito Y, Nakahira T and Iijima S 2002 *Phys. Rev. Lett.* **89** 155501
[20] Damnjanovic M, Vukovic T and Milosevic I 2002 *Eur. Phys. J.* B **25** 131
[21] Damnjanovic M, Milosevic I, Vukovic T and Sredanovic R 1999 *Phys. Rev.* B **60** 2728
[22] Kolmogorov A N and Crespi V H 2000 *Phys. Rev. Lett.* **85** 4727
[23] Wenning L and Muser M H 2001 *Europhys. Lett.* **54** 693
[24] Muser M H and Robbins M O 2000 *Phys. Rev.* B **61** 2335
[25] Donnet C, Martin J M, Le Mogne T and Belin M 1996 *Tribol. Lett.* **29** 123
[26] Buldum A and Lu J P 1999 *Phys. Rev. Lett.* **83** 5050
[27] Ni B and Sinnott S B 2001 *Surf. Sci.* **487** 87
[28] Frankland S J V, Caglar A, Brenner D W and Griebel M 2002 *J. Phys. Chem.* B **106** 3046
[29] Brenner D W 1990 *Phys. Rev.* B **42** 9458
[30] Mao Z G, Garg A and Sinnott S B 1999 *Nanotechnology* **10** 273
[31] Dong S R, Tu J P and Zhang X B 2001 *Mater. Sci. Eng.* A **313** 83
[32] Xu X J, Thwe M M, Shearwood C and Liao K 2002 *Appl. Phys. Lett.* **81** 2833
[33] Liao K and Li S 2001 *Appl. Phys. Lett.* **79** 4225
[34] Kuzumaki T, Hayashi T, Miyazawa K, Ichinose H, Ito K and Ishida Y 1998 *Mater. Trans. JIM* **39** 578
[35] Tuzun R E, Noid D W and Sumpter B G 1995 *Nanotechnology* **6** 64
[36] Zhang S L, Liu W K and Ruoff R S 2004 *Nano Lett.* **4** 293
[37] Kahn D and Lu J P 1999 *Phys. Rev.* B **60** 6535
[38] Xia Z and Curtin W A 2004 *Phys. Rev.* B **69** 233408
[39] Guo W, Guo Y, Gao H, Zheng Q and Zhong W 2003 *Phys. Rev. Lett.* **91** 125501
[40] Legoas S B, Colluci V R, Braga S F, Coura P Z, Dantas S O and Galvao D S 2003 *Phys. Rev. Lett.* **90** 055504
[41] Zheng Q S, Liu J Z and Jiang Q 2002 *Phys. Rev.* B **65** 245409
[42] Rivera J L, McCabe C and Cummings P T 2003 *Nano Lett.* **3** 1001
[43] Guo Y J, Karasawa N and Goddard W A 1991 *Nature* **351** 464
[44] Pan C, Sampson M P, Chai Y, Hauge R H and Margrave J L 1991 *J. Phys. Chem.* **95** 2944
[45] Gao G H, Cagin T and Goddard W A 1998 *Nanotechnology* **9** 184
[46] Gao G H, Cagin T and Goddard W A 1998 *Phys. Rev. Lett.* **80** 5556
[47] Tuzun R E, Noid D W, Sumpter B G and Merkle R C 1996 *Nanotechnology* **7** 241
[48] Rivera J L 2003 Molecular modeling at interfaces: phase equilibria of complex fluids and mechanical properties of nanostructures *PhD Thesis* University of Tennessee, Knoxville
[49] Tuckerman M E, Berne B J and Martyna G J 1991 *J. Chem. Phys.* **94** 6811
[50] Nose S 1984 *J. Chem. Phys.* **81** 511
[51] Tuckerman M E, Berne B J and Martyna G J 1992 *J. Chem. Phys.* **97** 1990
[52] Humphreys D D, Friesner R A and Berne B J 1994 *J. Phys. Chem.* **98** 6885
[53] Procacci P and Berne B J 1994 *J. Chem. Phys.* **101** 2421
[54] Hathorn B C, Sumpter B G, Noid D W and Barnes M D 2002 *Macromolecules* **35** 1102